THE JOURNAL OF PHYSICAL CHEMISTRY C

Article

Cite This: J. Phys. Chem. C 2019, 123, 17588−17597

pubs.acs.org/JPCC

A Split DNA Scaffold for a Green Fluorescent Silver Cluster

Chen He,[†,∥] Peter M. Goodwin,[‡] Ahmed I. Yunus,[†] Robert M. Dickson,*[,§] and Jeffrey T. Petty*[,†,∥]

[†]Department of Chemistry, Furman University, Greenville, South Carolina 29613, United States

[‡]Center for Integrated Nanotechnologies, Los Alamos National Laboratory, Mail Stop K771, Los Alamos, New Mexico 87545, United States

[§]School of Chemistry and Biochemistry and Institute for Bioengineering & Bioscience, Georgia Institute of Technology, Atlanta, Georgia 30332, United States

Supporting Information

ABSTRACT: Silver molecules are chromophores with diverse spectra and rich photophysics, and DNA strands act as ligands that develop specific molecular silver species. For example, $C_4AC_4T^*C_3GT_4$ selectively yields a Ag_{10}^{6+} fluorophore with $\lambda_{ex}/\lambda_{em}$ = 490/550 nm. This single-stranded DNA coordinates and protects the cluster, and its integrity was challenged by breaking the phosphodiester backbone at the innocuous T*. The resulting C_4AC_4T and C_3GT_4 fragments also develop the same Ag_{10}^{6+} fluorophore but only when all three components (two fragments + Ag) are present. This $C_4AC_4T/C_3GT_4/Ag_{10}^{6+}$ complex is favored by higher DNA concentrations and preferentially forms when hybridization forces C_4AC_4T and C_3GT_4 onto a shared DNA duplex. The C_4AC_4T/C_3GT_4 assembly reverses when the cluster photodegrades, which suggests that the cluster is labile. C_4AC_4T forms an alternate cluster at low temperatures, but C_3GT_4 recovers the λ = 490 nm fluorophore at higher temperatures. Thus, the reciprocal interactions between the host DNA strands and the cluster adduct combine to create a highly specific, split-DNA fluorescent Ag cluster capable of sensing target DNA sequences with high specificity and on−off contrast.

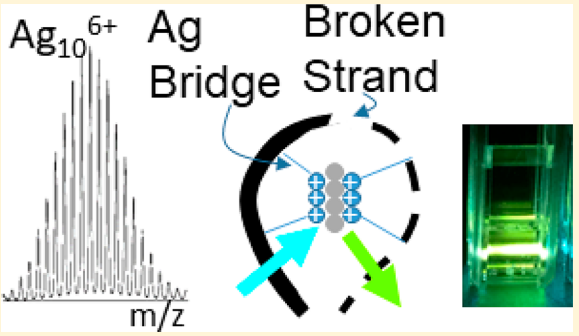

INTRODUCTION

Reduced, multinuclear silver clusters exhibit strong optical absorption because their metal-like valence electrons move between discrete electronic states.[1−4] Bare silver clusters with different stoichiometries and charges absorb and fluoresce throughout the visible spectral range in cryogenic matrices and in the gas phase, but they decompose outside these pristine environments.[5−7] However, this instability is largely tempered when silvers coordinate with short, single-stranded DNA, and the resulting conjugates form a new class of biosensing and imaging fluorophores with many advantages.[8−12] Oligonucleotides with $\gtrsim$10 nucleobases bind and sequester limited numbers of ∼10 silvers, often yielding monodisperse adducts.[13−17] DNA strands are scaffolds that assemble around, template formation of, and protect their embedded fluorescent silver cluster adducts.[18−21] Beyond acting simply as a protecting layer, DNA strands nucleate and stabilize emissive silver clusters through their interactions with both Ag^+ and Ag^0. As a result, the spectra and photophysics of the composite cluster are strongly influenced by both DNA structure/sequence and metal cluster size/electronic structure.[22] Strands with different sequences control the number and geometry of the silver atoms and thereby tune the cluster spectra from the near-ultraviolet to the near-infrared.[23−25] Strands with different sequences and structures determine cluster size, geometry and, therefore, electronic structure. Thus, cluster color and brightness are drastically altered between hybridized vs single-stranded oligonucleotides to develop cluster adducts with up to ∼1000-fold emission."[26,27] Coupled structural and spectral changes are the foundation of optical biosensors that activate and "turn on" when target complementary strands hybridize with a sensing domain in the DNA−cluster conjugate.[10] Even greater gains in sensitivity are achieved via dark electronic states that can be optically depopulated.[28] These μs-lived states can be selectively excited via near-infrared lasers that enhance the visible cluster emission against the autofluorescence background.[29,30] Building on these advantages, this paper demonstrates that a split-DNA construct and a green fluorescent silver cluster unite to form a single emissive DNA−cluster conjugate, which leads to a two-stranded fluorescence complementation sensor.

Oligonucleotides are multidentate ligands that coordinate and encapsulate molecular silver clusters via their nucleobases.[8,31] As measured with isothermal titration calorimetry, the electron-rich nucleobase heteroatoms within the DNA strands bind silver ions with μM dissociation constants, and their affinity with silver clusters is governed by their basicity.[18,22,32−34] It is the interactions of both cationic and

Received: April 22, 2019
Revised: June 26, 2019
Published: June 26, 2019

DOI: 10.1021/acs.jpcc.9b03773
J. Phys. Chem. C 2019, 123, 17588−17597

neutral silvers with the multidentate DNA that makes DNA such a good template for emissive Ag cluster formation. Multiple nucleobases anchor a silver cluster, and the DNA length sets the number of nucleobases. For example, $(C_2A)_x$ sequences with $x \geq 6$ have the requisite length to stabilize a specific silver cluster fluorophore.[35] Single-stranded oligonucleotides are flexible heteropolymers whose primary sequence and secondary structure establish unique three-dimensional binding sites for specific clusters. Our studies compare a contiguous single-stranded oligonucleotide and its corresponding pair of fragments. These constructs have identical sequences and thus form the same cluster. However, the bifurcated scaffold reveals key interactions within the DNA−silver cluster complex.

Our studies began with $C_4AC_4TC_3G$ because it preferentially develops a silver cluster with $\lambda_{ex}/\lambda_{em}$ = 490/550 nm.[36] The coordination environment for this cluster was probed by substituting, modifying, or eliminating nucleobases, and stark differences were revealed. Specifically, any excision of cytosine destroys the cluster, whereas the lone thymine could be excised and replaced by other nucleobases as well as an ethylene glycol without altering the cluster spectra or photophysics. We targeted this seemingly innocuous thymine by cleaving the covalent phosphodiester backbone at this site. For these studies, we chose $C_4AC_4TC_3GT_4$ because its two similarly sized fragments—C_4AC_4T and C_3GT_4—can be commercially synthesized, and the additional thymines do not significantly perturb the cluster.[36] We studied this DNA fragment pair as a silver cluster scaffold. Optical and mass spectra identify a C_4AC_4T/C_3GT_4 complex with a specific cluster that also develops with the parent $C_4AC_4TC_3GT_4$ strand. Higher DNA concentrations favor the aggregate complex, which develops when hybridization concentrates the strands onto a shared DNA template. Photolysis reverses the assembled complex by selectively exciting and breaking the silver network that links the DNA fragments. Low temperature regulates the DNA−cluster formation by controlling how the nucleobases in C_4AC_4T and C_3GT_4 coordinate silvers. These experiments collectively suggest how the DNA fragments collectively template their fluorescent silver cluster adduct.

METHODS

Synthesis. Desalted oligonucleotides were purchased from Integrated DNA Technologies and dissolved in deionized water. The complete list of DNA sequences is provided in the Supporting Information (Table S1). The molar extinction coefficients of these oligonucleotides were calculated on the basis of the nearest-neighbor approximation, and the DNA concentrations were determined using the Lambert−Beer law.[37]

Buffer solutions controlled the pH and electrostatically screened the negatively charged DNA backbone.[38,39] In a typical synthesis, a 150 μL sodium cacodylate buffer solution (5 mM, pH 6.95) with 37.5 μM $C_4AC_4TC_3GT_4$ and 300 μM $AgNO_3$ (8 mol equiv per DNA) was heated (∼80 °C) for 5 min and then cooled to room temperature. This sample was chemically reduced with $NaBH_4$ (4 mol equiv per DNA) into the reaction mixture and vortexed for 1 min. The solution became yellow due to the formation of Ag clusters. This solution was then treated with 400 psi of O_2 for 2−3 h to eliminate alternate clusters,[40] and the final product was stored at 4 °C before use.

The T* in $C_4AC_4T^*C_3GT_4$ was replaced by uracil and enzymatically excised with uracil-DNA glycosylase (New England BioLabs).[35] The reaction used 15 μL of 1 mM oligonucleotide, 7.5 μL of enzyme (3.5 units), and 5 μL of 10× reaction buffer (from supplier but without dithiothreitol, DTT) in a total volume of 50 μL. The resulting solution was incubated at 37 °C for >1 h and subsequently dialyzed against water. The extinction coefficient for the resulting strand was calculated by the nearest-neighbor method after accounting for the excised nucleobase.

The synthetic procedures for the split and colocalized silver clusters were adapted from the ones for their intact analogues described above. To synthesize the split clusters, we first prepared a 150 μL sodium cacodylate buffer solution (5 mM, pH 6.95) that contained 37.5 μM C_4AC_4T (II), 37.5 μM C_3GT_4 (III), and 300 μM $AgNO_3$ (8 mol equiv per II). The mixture was heated to ∼80 °C for 5 min and then cooled with tap water, as described above. The reaction mixture was reduced with $NaBH_4$ (4 mol equiv per II) and vortexed for 1 min. The resulting yellow solution was then treated with 400 psi of O_2 at 40 °C for ∼2 h in a high-pressure reactor, and the final product was stored at 4 °C before use.

To synthesize colocalized silver nanoclusters, we first prepared a 300 μL sodium cacodylate buffer solution (5 mM, pH 6.95) that contained 10.0 μM of each hybridizing component. The sample was heated to ∼90 °C in 1 L of water for 30 min and then cooled slowly to 0 °C. We mixed $AgNO_3$ (8 mol equiv per strand) into the cooled DNA solution, injected $NaBH_4$ (4 mol equiv per strand) 10 min later, vortexed the solution for 1 min, and cooled it again immediately using an ice bath. The resulting solution was then treated with 400 psi of O_2 at 0 °C for ∼2 h in a high-pressure reactor, and the final product was stored at 4 °C before use. Samples were photolyzed with 476 nm irradiation from an argon ion laser at an intensity of 1 W/cm^2 for ∼30 min.

Optical Characterization. Absorption spectra of DNA−Ag cluster conjugates were collected on a Cary 50 UV−vis spectrophotometer (Varian), and steady-state emission spectra were collected on a Fluoromax-3 spectrofluorometer (Jobin-Yvon Horiba). Fluorescence quantum yields (QYs) were measured using fluorescein as the standard (QY = 95%).[41] Circular dichroism (CD) spectra were acquired on a DSM 17 CD spectrophotometer (Olis).

Time-correlated single photon counting used a pulsed 470 nm laser (PicoQuant) at a pulse repetition rate of 10 MHz. The excitation beam was vertically polarized, and its power was adjusted to achieve a detection rate of fewer than 5 photons per 100 pulses (<5 × 10^5 Hz). The emission was collected at a right angle with the emission polarizer set to the magic angle (∼55°) and spectrally filtered using a 525 ± 20 nm bandpass filter. The instrument response function (IRF) was collected using colloidal silica (Aldrich), and its fwhm was ∼150 ps. The kinetics of fluorescence decay was extracted through IRF convolution fitting of the measured decay (FluoFit). The fluorescence anisotropy measurements were made using vertically (V) polarized excitation along with vertically (V) or horizontally (H) polarized emission. The *G*-factor accounts for the detection efficiency of vertically and horizontally polarized emission, and it was ∼1 for our filter-based instrument.[42] The fluorescence decays under two different configurations, $I_{VV}(t)$ and $I_{VH}(t)$, were convolved with the IRF

DOI: 10.1021/acs.jpcc.9b03773
J. Phys. Chem. C 2019, 123, 17588−17597

to calculate the anisotropy decay, $r(t)$, and rotational correlation time, τ_c, using the following expression (FluoFit):

$$r(t) = \frac{I_{VV}(t) - I_{VH}(t)}{I_{VV}(t) + 2I_{VH}(t)} = r(0)e^{-t/\tau_c}$$

The volume, V, and the hydrodynamic radius (assuming a quasi-spherical shape), R, of the cluster were calculated using the following expressions

$$V = \frac{\tau_c k_B T}{\eta}$$

$$R = \left(\frac{3V}{4\pi}\right)^{1/3}$$

where $k_B = 1.38065 \times 10^{-23}$ J/K is the Boltzmann constant, $T = 298.15$ K is the temperature, and $\eta = 0.89$ mPa·s is the viscosity of water at 25 °C.

Fluorescence correlation spectroscopy (FCS) studies were performed using an apparatus similar to that described in our earlier reports.[43] Briefly, samples were excited at 488 nm, and autocorrelation analysis of the fluorescence fluctuations ($G(\tau)$) was resolved into diffusive ($g_D(\tau)$) and excited state ($g_{ES}(\tau)$) contributions

$$G(\tau) = 1 + \frac{1}{N} g_D(\tau) g_{ES}(\tau)$$

where $g_D(\tau)$ is based on a 3-D Gaussian model

$$g_D(\tau) = \left(1 + \frac{\tau}{\tau_d}\right)^{-1} \left(1 + \left(\frac{\omega}{z}\right)^2 \left(\frac{\tau}{\tau_d}\right)\right)^{-1/2}$$

and

$$g_{ES}(\tau) = 1 + \frac{F}{1 - F} e^{-\tau/\tau_{ES}}$$

In these equations, τ is the lag time, N is the average number of fluorescent species in the probe volume, ω is the transverse radius of the probe volume, z is the height of the probe volume, τ_d is the lag time at which the diffusive autocorrelation amplitude has decayed to approximately one-half of its maximum value, $G(0)$, F is the fractional occupancy of the dark state, and τ_{ES} is the net correlation time for dark state shelving. The aspect ratio z/ω was determined using fluorescein and set to 6.7 for fitting the DNA–Ag cluster fluorescence intensity autocorrelations. We used the occupancy (N) of the probe volume to determine the extinction coefficient of the clusters. The size of the FCS probe volume was determined to be ~1 fL from the fluorescence autocorrelation recorded on fluorescein in water.[44]

Mass Spectrometry. The stoichiometry and charge of DNA–Ag cluster conjugates were characterized by electrospray ionization mass spectrometry (Q-TOF G2-S, Waters). Samples were diluted with deionized water to ~0.3 μM and were infused via a syringe pump operated at a flow rate of 20 μL/min. The spectra were collected in the negative ion mode with a capillary voltage of −2.7 kV, a sampling cone voltage of −15 V, an extraction cone voltage of 10 V, a cone gas flow of 45 L/h, and a desolvation gas flow of 450 L/h. The source temperature was 80 °C, and the desolvation temperature was 150 °C. Mass calibration was performed using aggregates of sodium formate in the $400 < m/z < 2000$ range. The spectra were analyzed using MassLynx V4.1.

RESULTS

A Ternary $C_4AC_4T/C_3GT_4/Ag_{10}^{6+}$ Complex. Our studies were based on $C_4AC_4TC_3GT_4$ that preferentially forms a $\lambda_{ex}/\lambda_{em}$ = 490/550 nm fluorophore (Figure 1). This sequence can

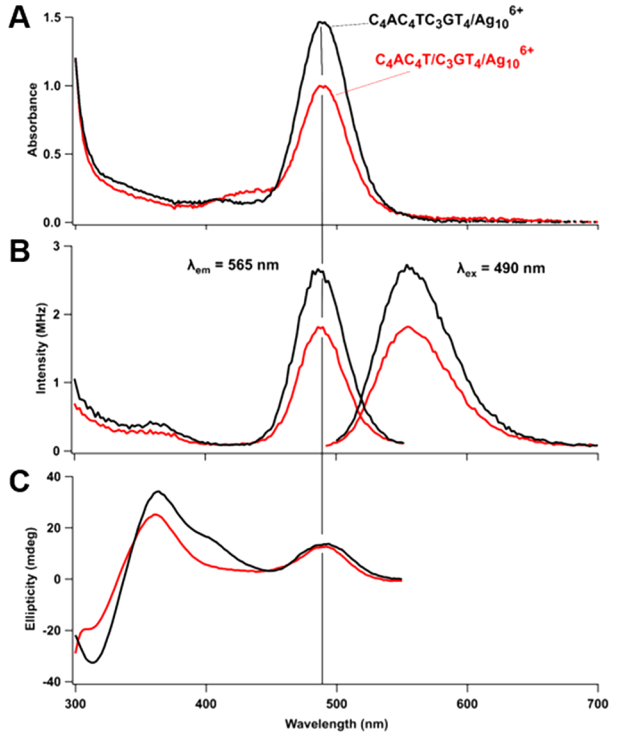

Figure 1. Absorption (A), fluorescence (B), and circular dichroism (C) spectra of Ag_{10}^{6+} synthesized using $C_4AC_4TC_3GT_4$ (black) and C_4AC_4T/C_3GT_4 pair (red). The vertical line at λ = 490 nm highlights the match between the spectra.

be divided, and the breakpoint was identified enzymatically. The central thymine was replaced with a uracil, which was then excised using uracil-DNA glycosylase.[35,45] The resulting $C_4AC_4DC_3GT_4$ has an abasic site, D, that preserves the phosphodiester backbone, and this modified strand forms the same λ = 490 nm cluster (Figure S1). Thus, this thymine does not bind the cluster and may lie in a flexible, folded region of the strand, as also found in the analogous $C_4AC_4TC_3G$ strand.[36,46] We decided to break the strand at this site, and the resulting C_4AC_4T/C_3GT_4 pair and the parent $C_4AC_4TC_3GT_4$ form the same chromophore with an identical absorption maximum and line width (Figures 1A and S2A). The single absorption band suggests that both types of scaffolds favor only one chromophore.[40] Neither C_4AC_4T nor C_3GT_4 alone produces this species (Figure S3). Thus, despite severing the strand at the thymine base, C_4AC_4T and C_3GT_4 mimic the intact $C_4AC_4TC_3GT_4$ scaffold and collectively coordinate the λ = 490 nm cluster. However, the site of interruption is important; when $C_4AC_4TC_3GT_4$ was alternatively severed at the adenine, the $C_4A/C_4TC_3GT_4$ pair yielded a different cluster (Figure S4).

A reduced silver cluster binds with both $C_4AC_4TC_3GT_4$ and the C_4AC_4T/C_3GT_4 pair, and these complexes were analyzed by electrospray ionization mass spectrometry (Figure 2). DNA molecular formulas as well as cluster stoichiometries and charges were determined from the isotopic fine structure of the different charge states (Figure 2C).[15,18,47,48] The intact

DOI: 10.1021/acs.jpcc.9b03773
J. Phys. Chem. C 2019, 123, 17588–17597

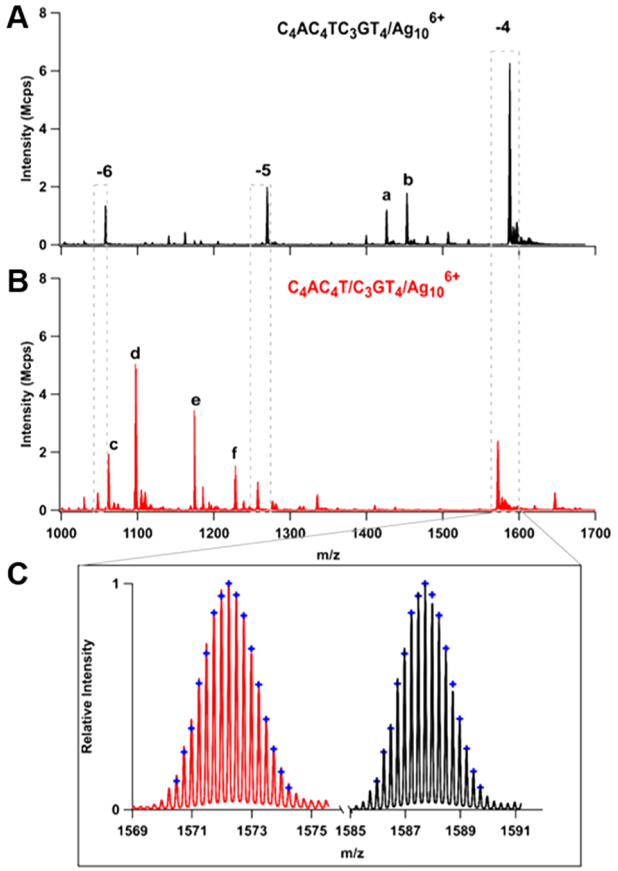

Figure 2. Mass:charge spectra of $C_4AC_4TC_3GT_4$ (A) and C_4AC_4T/C_3GT_4 (B) complexes with Ag_{10}^{6+} in −6, −5, and −4 charge states (CS, dashed boxes). Complexes with Ag^+ alone are also marked: "a" and "b" are $C_4AC_4TC_3GT_4$ with 4 and 5 Ag^+ (−4 CS), respectively; "c" and "d" are C_4AC_4T with 3 and 4 Ag^+ (−3 CS), respectively; and "e" and "f" are C_3GT_4 alone and with 1 Ag^+ (−2 CS), respectively. (C) Isotopologue distributions for $C_4AC_4TC_3GT_4/Ag_{10}^{6+}$ (black) and $C_4AC_4T/C_3GT_4/Ag_{10}^{6+}$ (red) complexes (−4 CS). The blue ticks describe isotopologue distributions predicted on the basis of $C_{169}H_{222}O_{110}N_{53}P_{17}Ag_{10}$ (A) and $C_{169}H_{223}O_{108}N_{53}P_{16}Ag_{10}$ (B).

$C_4AC_4TC_3GT_4$ almost exclusively forms a 10-silver complex with 6 Ag^+ and 4 Ag^0 (Figure 2A). In relation to this $C_4AC_4TC_3GT_4/Ag_{10}^{6+}$, C_4AC_4T and C_3GT_4 collectively form the analogous Ag_{10}^{6+} complex. This $C_4AC_4T/C_3GT_4/Ag_{10}^{6+}$ is lighter because the C_4AC_4T/C_3GT_4 pair lacks the 5′-phosphate that links the parent $C_4AC_4TC_3GT_4$ strand (Figures 2C and S5). Both types of DNA also bind Ag^+ alone, but Ag_{10}^{6+} is the only silver cluster/chromophoric species in the mass spectra.[2] Subsequently, photochemistry further links the Ag_{10}^{6+} cluster to the λ = 490 nm chromophore.

The electronic and mass spectra suggest that the C_4AC_4T and C_3GT_4 fragments are rejoined by Ag_{10}^{6+}, and this three-component emitter was investigated by time-resolved fluorescence anisotropy (Figure S6). The embedded cluster is a fluorophore with $\lambda_{ex}/\lambda_{em}$ = 490/550 nm, and such species have well-defined absorption transition dipoles that can be selectively excited with polarized light (Figure 1B).[49] The polarized emission dephases with rotational correlation times (τ_r) that depend on the molecular volume and are dominated by the shape of the bulky DNA host.[42] As a reference, the $C_4AC_4TC_3GT_4/Ag_{10}^{6+}$ complex has a value of τ_r = 2.55 ± 0.02 ns, and this time constant reflects the rate of tumbling by the DNA host, as found with similar strands labeled by organic dyes.[50,51] The C_4AC_4T/C_3GT_4 complex with Ag_{10}^{6+} has an identical value of τ_r = 2.53 ± 0.06 ns. Thus, matching τ_r values suggest that C_4AC_4T and C_3GT_4 reassemble with Ag_{10}^{6+} and mimic the overall shape of $C_4AC_4TC_3GT_4/Ag_{10}^{6+}$. Therefore, the covalent break in $C_4AC_4T/C_3GT_4/Ag_{10}^{6+}$ seems innocuous, so we now probe the cluster coordination environment.

The DNA-bound Ag_{10}^{6+} has a circular dichroism peak at 490 nm that coincides with its absorption band, and the inherent circular dichroism (κ) was derived from the ellipticity normalized by the absorbance (Figure 1C).[52] Similar κ values of 0.3 × 10^{-3} and 0.4 × 10^{-3} with the C_4AC_4T/C_3GT_4 and $C_4AC_4TC_3GT_4$ scaffolds, respectively, suggest that a similar set of chiral nucleosides coordinates Ag_{10}^{6+} in both scaffolds.[53] Comparable κ values have also been measured for other DNA sequences.[54,55]

The selectivity of C_4AC_4T/C_3GT_4 for binding Ag_{10}^{6+} was assessed by measuring emission spectra with varied excitation wavelengths (Figure S7).[56] The emission spectra are independent of excitation wavelength for λ_{ex} = 440−540 nm. Furthermore, the absorption profile overlaps with the excitation spectrum (Figure S2B), thus supporting a dominant fluorophore. In line with the metal-centered emission from other DNA-bound chromophores, fluorescence quantum yields (ϕ_f) of 22 ± 3 and 28 ± 4% and average lifetimes (τ_f) of 1.6 and 1.9 ns with $C_4AC_4T/C_3GT_4/Ag_{10}^{6+}$ and $C_4AC_4TC_3GT_4/Ag_{10}^{6+}$, respectively, signify similar coordination environments in the two types of DNA scaffolds (Figure S8 and Table S2).[23,36,57]

Fluorescence correlation spectroscopy identified dark excited electronic states with ∼μs lifetimes that provide a longer temporal snapshot of the coordination environment.[28,58,59] Electronically excited $C_4AC_4T/C_3GT_4/Ag_{10}^{6+}$ complexes cross into a dark state, of which the steady-state population increased and the lifetime decreased with increasing laser irradiance, as observed in other DNA−cluster fluorophores (Figure S9).[25,60] Similar decay rates and populations between the intact and split DNA scaffolds support their similar coordination environments. The correlation functions also yield the extinction coefficients. The amplitude of the diffusive portion of the correlation function was extrapolated to zero lag time and is inversely proportional to the number of fluorophores in the probe volume. The resulting statistically averaged concentrations, along with the absorbances from the bulk solutions, determined extinction coefficients of 48,000 ± 5000 and 43,000 ± 7000 M^{-1} cm^{-1} at 488 nm for clusters with intact and split DNA strands, respectively. Comparable extinction coefficients have also been reported for other green-emitting silver cluster conjugates with DNA.[43]

Steering the $C_4AC_4T/C_3GT_4/Ag_{10}^{6+}$ Assembly. Higher DNA concentrations favor the $C_4AC_4T/C_3GT_4/Ag_{10}^{6+}$ complex. When the amount of C_3GT_4 increases from 0.5 to 10 mol equiv per C_4AC_4T strand, both the cluster absorbance and concentration increase, on the basis of parallel absorption and fluorescence correlation spectroscopy studies (Figure S10). Despite the 10-fold excess concentration, C_3GT_4 does not disrupt the Ag_{10}^{6+} cluster, so it may be the weaker partner in the complex. Instead of letting the strands naturally assemble, an alternative strategy guided the reaction by specifically forcing C_4AC_4T and C_3GT_4 together. We wanted to understand if these constrained sequences would still assemble and create the Ag_{10}^{6+} cluster. Both strands were appended with sequences that hybridized either with each other or with two

DOI: 10.1021/acs.jpcc.9b03773
J. Phys. Chem. C 2019, 123, 17588−17597

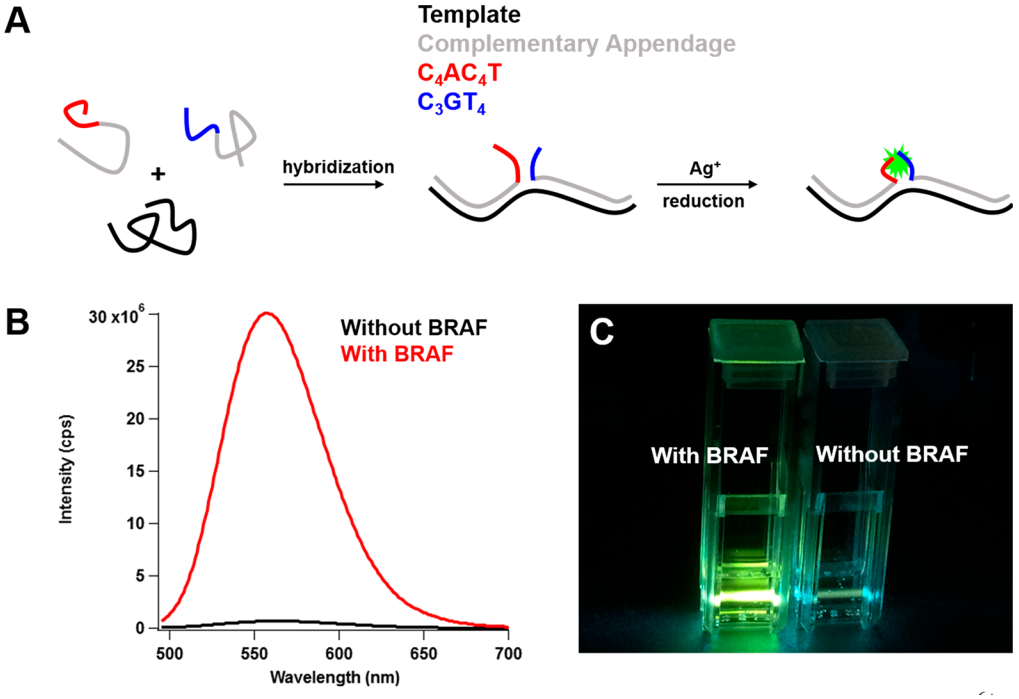

Figure 3. (A) Schematic representation of a quaternary duplex/C_4AC_4T/C_3GT_4/Ag_{10}^{6+} conjugate. The color of each component matches the color in Table S1. (B, C) Fluorescence spectra and photograph of clusters synthesized with or without a BRAF template.

halves of a shared DNA template (Figures 3 and S11). The latter constructs were based on a segment of the proto-oncogene B-Raf (BRAF) or the DNA sequence of a subtype of Influenza A virus (H1N1).[26] Our studies utilized four characteristics of canonical DNA duplexes. First, the >20-nucleotide appendages form stable duplexes with their complements, so the appended C_4AC_4T and C_3GT_4 are pulled together when the duplex anneals (Figure 3A).[61] Second, the short duplexes locally concentrate the C_4AC_4T and C_3GT_4 and promote DNA assembly. Third, the complementary strands are polar, so C_4AC_4T and C_3GT_4 can be attached to the same 3′−5′ end or opposite 5′−5′ ends of antiparallel duplexes to control their proximity.[62] Fourth, the strands can readily be extended with inert thymines to offset the C_4AC_4T and C_3GT_4 positions.

We designed a set of experiments to probe the quaternary duplex/C_4AC_4T/C_3GT_4/Ag_{10}^{6+} complexes. C_4AC_4T and C_3GT_4 only assemble and form Ag_{10}^{6+} when they are on the same end of the duplex, and they cannot bypass this stiff, intervening duplex (Figure S12a and b). Being strongly bound to each other, the duplex is an inert platform whose sequence does not influence C_4AC_4T and C_3GT_4, presumably because base pairs occlude silver clusters (Figures S11 and S12).[21] Increasing amounts of complement correspondingly increases the cluster yield, which indicates that the duplex concentrates the reactants and guides the reaction (Figure S12c and d). By incorporating a flexible eight-thymine spacer, even offset C_4AC_4T and C_3GT_4 sequences still assemble and nucleate the cluster (Figure S12a and c). Reversing the CCCGTTTT sequence to TTTTGCCC, however, produced a different cluster instead, so specific sequences are still needed even though the two strands have the same numbers and types of nucleobases (Figures S12a and d). Thus, colocalizing and concentrating the strands promotes C_4AC_4T/C_3GT_4-templated formation of the emissive Ag_{10}^{6+} adduct. Analogous to DNA-templated organic reactions, the silver clusters form via constructs that control the strand concentrations, positions, and orientations.[63,64]

A Photoexcited Ag_{10}^{6+}. C_4AC_4T and C_3GT_4 combine to jointly template the final emissive Ag_{10}^{6+} cluster, but unlike the emitter formed from the full-length DNA strand, this three-component complex is broken through photolysis. When irradiated, silver clusters can be fluxional and labile, as illustrated by Ag_2 with a bond dissociation energy of 1.7 eV (750 nm).[65] Ag_{10}^{6+} also appears to photodissociate upon extensive irradiation, but its path depends on its host DNA. $C_4AC_4TC_3GT_4$/Ag_{10}^{6+} was selectively excited via its λ = 490 nm transition, and this feature was replaced by a new band with λ_{max} ∼ 340 nm. Furthermore, the Ag_{10}^{6+} adduct in the mass spectrum was eliminated to yield more oxidized products—largely Ag_8^{6+} with smaller amounts of Ag_9^{7+}, Ag_7^{5+}, and $(Ag^+)_6$ adducts (Figure 4A).[66] Prior studies suggest that even numbers of reduced silvers are favored, while the numbers of oxidized silvers can vary.[35,67] These spectra suggest that irradiation selectively excites and partially degrades the Ag_{10}^{6+} cluster. The Ag_{10}^{6+} within C_4AC_4T/C_3GT_4 was also irradiated, and it likewise loses its 490 nm absorption in lieu of a shoulder at ∼340 nm. However, no remnant of the silver-linked DNA pair remains (Figure 4B). These results suggest that the cluster links the two strands, which is consistent with cross-linking and folding in a related intact strand.[36]

Temperature Reveals Distinct Ligands. Temperature changes the course of the reaction and reveals differences between the C_4AC_4T and C_3GT_4 ligands. Two samples were prepared either with only C_4AC_4T or with a 1:5 mixture of C_4AC_4T and C_3GT_4, and these samples were combined with Ag^+ and chemically reduced at 0 °C (Figure 5). A species developed with λ_{max} ∼ 430 nm and lower emission relative to the λ = 490 nm cluster (Figure S13), but this new chromophore does not form with C_3GT_4 alone (Figure S3). The two samples were then heated to 45 °C. While the cluster with only C_4AC_4T decomposed, the same cluster with both

DOI: 10.1021/acs.jpcc.9b03773
J. Phys. Chem. C 2019, 123, 17588−17597

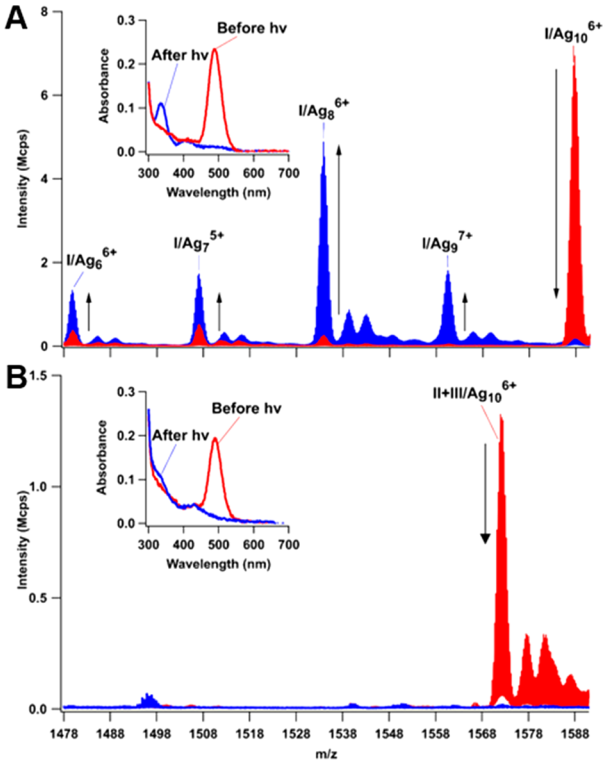

Figure 4. Mass:charge spectra of $C_4AC_4TC_3GT_4$ (A) and C_4AC_4T/C_3GT_4 (B) labeled with the Ag_{10}^{6+} cluster before (red) and after (blue) irradiation at 476 nm. The insets show the corresponding absorption spectra.

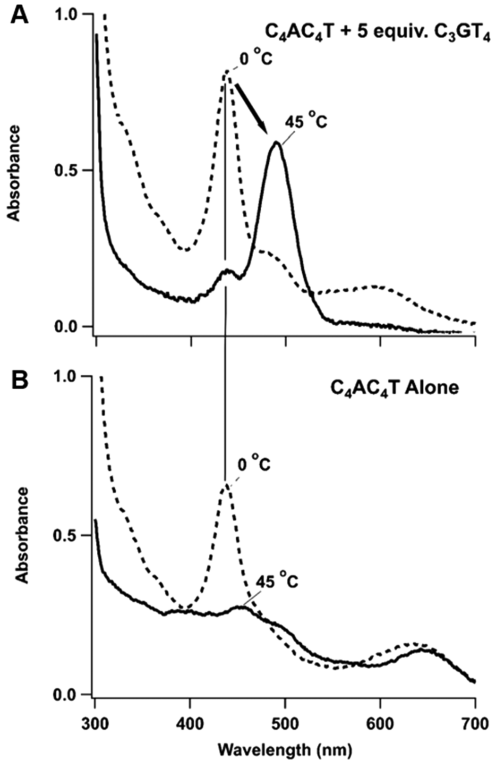

Figure 5. Absorption spectra of C_4AC_4T–silver cluster complexes with λ_{max} = 430 nm at 0 °C (dashed) and 45 °C (solid). The spectra were acquired with C_4AC_4T alone (A) and C_4AC_4T with 5 equiv of C_3GT_4 (B).

C_4AC_4T and C_3GT_4 converted to the 490 nm chromophore (Figure 5). These observations suggest that C_4AC_4T preferentially binds silvers at low temperatures and kinetically traps the alternate 430 nm cluster, despite the large excess of C_3GT_4. However, this cluster decomposes without C_3GT_4. Thus, the two strands have distinct roles—C_4AC_4T alone preferentially nucleates a different silver cluster, while it can pair with C_3GT_4 at higher temperatures to specifically stabilize the Ag_{10}^{6+} adduct.

DISCUSSION

The single-stranded $C_4AC_4TC_3GT_4$ selectively develops a green fluorescent silver cluster, but this oligonucleotide can be broken into two fragments that collectively form the same cluster. We now consider the insights and opportunities afforded by this bifurcated DNA template. We discuss how the breakpoint was chosen on the basis of an innocuous site within the contiguous parent strand. The resulting set of fragments naturally reassembles, but their assembly can also be directed. We thus developed a two-stranded fluorescence complementation reporter in which hybridization pulls the fragments together to activate the cluster formation and emission. The DNA assembly can be reversed by photolysis. Within the complex, the two DNA fragments are distinct polydentate ligands with dominant and subservient roles in the aggregate complex.

The C_4AC_4T/C_3GT_4 pair yields the same cluster chromophore as the intact stand, which suggests that it is a supramolecular assembly (Figures 1 and 2). Intact oligonucleotides can fold into hairpin-like structures to coordinate silvers, and key signatures of intermolecular DNA–silver cluster–DNA complexes have been previously elucidated.[16,19,22,27,68,69] They have specific numbers and arrangements of the constituent strands. For example, derivatives of $C_3AC_3AC_3TC_3A$ dimerize and form a cluster with near-infrared absorption and emission. The strands have antiparallel orientations and do not fully overlap. Even higher-order dimer-of-dimer structures have been identified in solid- and solution-phase studies of A_2C_4.[70] The dimeric subunits have parallel A_2C_4 orientations, and the two dimers have antiparallel orientations in which adenines swap between the two domains. Furthermore, supramolecular DNA–cluster constructs are molecules with particular numbers of silvers. The $(C_3AC_3AC_3TC_3A)_2$ and $(A_2C_4)_4$ aggregates bind 20 and 19 silvers, respectively. We suggest that the C_4AC_4T/C_3GT_4 pair is an analogous complex, but it is distinctive because it is a heterodimer. We subsequently discuss how the two different ligands open the possibility in tuning the cluster environment.

The quaternary duplex/$C_4AC_4T/C_3GT_4/Ag_{10}^{6+}$ complex shows that DNA strands can both form clusters and direct cluster synthesis (Figure 3). Such constructs link specific biomolecular recognition with cluster formation and could serve as a model for optical biosensors. For example, fluorescence complementation sensors have been developed by dissecting green fluorescent proteins and DNA aptamers at sacrificial loops.[71−73] The resulting fragments are joined by biomolecules that associate and fuse the two fragments. As another example, dark DNA–cluster complexes gain >1000× emission when an activator strand hybridizes with the target.[10,74] Such sensors offer a sensitive and cost-effective alternative to molecular beacons and have been used in a wide range of applications, and an improved understanding of their

DOI: 10.1021/acs.jpcc.9b03773
J. Phys. Chem. C 2019, 123, 17588−17597

mechanism of fluorescence enhancement could expand their applicability.[75−77]

The Ag_{10}^{6+} chromophore is somewhat labile as the complex dissociates upon continuous cluster photoexcitation (Figure 4). This result highlights interactions within the two strand−cluster complex. Previous X-ray spectroscopy and diffraction studies suggest that the silvers with DNA−cluster complexes can segregate.[55,70,78] These results suggest that the Ag_{10}^{6+} cluster within the $C_4AC_4T/C_3GT_4/Ag_{10}^{6+}$ complex may cross-link the two strands.[22,79−86] Various silver species that disperse within their DNA hosts are further supported by electronic spectra and theoretical calculations.[22,48,54,67,87,88] As silvers are known to bind to DNA nucleobases and the spacing between DNA bases closely matches Ag−Ag metallic bond distances, DNA provides an excellent coordination environment for emissive Ag cluster formation.[70] Further, our photolysis studies suggest that the silver cluster may link the fragments, as photoexcitation breaks the two-strand complex apart. Importantly, coupled cluster excitation and DNA dissociation suggest the possibility of photoreversible complementation.[72]

Relative to C_4AC_4T that preferentially develops a λ = 430 nm cluster, C_3GT_4 appears to be a weaker ligand that requires higher concentrations to yield the two-stranded complex for the λ = 490 nm fluorophore (Figure 5). Other dominant/subservient DNA pairs have also been characterized through thermodynamic and spectroscopic studies.[27,77] The dominant strands are longer oligonucleotides that integrate two functions—one end develops a dim silver cluster chromophore, and the other end hybridizes with shorter, complementary strands.[18,27,55,78] These single-stranded oligonucleotides encapsulate and stabilize the silvers within their cluster adduct.[18,22] The subservient strands are the complements because they must have sufficient length and affinity to intrude into the folded complexes. Once hybridized, these complements only change the cluster shape and thereby activate the cluster emission.[78] We suggest that C_3GT_4 acts similarly by fine-tuning the cluster environment to favor the $\lambda_{ex}/\lambda_{em}$ = 490/550 nm cluster. The limited length of this strand suggests that systematic changes in its sequence could further modulate the cluster spectra and photophysics.[36]

CONCLUSION

$C_4AC_4T/C_3GT_4/Ag_{10}^{6+}$ reveals concepts that further our understanding of DNA−silver cluster fluorophores and sensors. This complex depends on reciprocal interactions. On one hand, Ag_{10}^{6+} is not a passive adduct that resides in a DNA binding pocket, but the recent first crystal structure of an emissive DNA−Ag cluster clearly shows that the complex depends on both nucleobase−Ag and Ag−Ag interactions and that flexibility in the encapsulating DNA strands is crucial for cluster formation.[70] On the other hand, the DNA strands are multidentate ligands, and different constituent strands in a heterodimer scaffold could have distinct roles. We focused on a specific sequence/cluster conjugate, but our results could be translated to other DNA−cluster systems. Viable breaks in their phosphodiester backbones could be identified by excising innocuous nucleobases, such as thymines. The resulting fragments could also be localized, oriented, and assembled using DNA hybridization, thus expanding the toolset of fluorescence complementation sensors. In summary, bifurcated DNA pairs suggest new paths to understand and develop the distinctive optical properties of DNA-based silver cluster chromophores.

ASSOCIATED CONTENT

Supporting Information

The Supporting Information is available free of charge on the ACS Publications website at DOI: 10.1021/acs.jpcc.9b03773.

A total of 2 tables and 13 figures related to the structural analyses and spectroscopic characterizations of DNA−silver cluster complexes: a table that describes the 16 DNA sequences used in this work; a table that summarizes the fluorescence lifetimes of the cluster with $C_4AC_4TC_3GT_4$ and C_4AC_4T/C_3GT_4; absorption spectra of $C_4AC_4TC_3GT_4$ without and with an abasic site; normalized absorption and excitation spectra of $C_4AC_4TC_3GT_4$ and C_4AC_4T/C_3GT_4 complexes with Ag_{10}^{6+}; absorption spectra of clusters synthesized with C_4AC_4T alone, C_3GT_4 alone, and C_4AC_4T/C_3GT_4 together; absorption spectra of clusters synthesized with C_4AC_4T/C_3GT_4 vs $C_4A/C_4TC_3GT_4$; schematic description of the differences in molecular formulas of $C_4AC_4TC_3GT_4$ and C_4AC_4T/C_3GT_4; representative kinetic traces of the fluorescence anisotropy decay of DNA−silver cluster adducts; contoured emission/excitation spectra of the $C_4AC_4T/C_3GT_4/Ag_{10}^{6+}$ fluorophore; representative fluorescence decay of $C_4AC_4T/C_3GT_4/Ag_{10}^{6+}$ with multiexponential fits; fluorescence correlation functions with increasing irradiance; absorption spectra and fluorescence correlation functions with increasing relative amounts of C_3GT_4/C_4AC_4T; schematic representation of C_4AC_4T and C_3GT_4 strands colocalized on seven duplex DNA templates and absorption spectra of their silver cluster adducts; emission spectra and integrated emission intensity of clusters synthesized with an increasing amount of template DNA; fluorescence spectra of 430 vs 490 nm clusters (PDF)

AUTHOR INFORMATION

Corresponding Authors

*E-mail: jeff.petty@furman.edu.

*E-mail: robert.dickson@chemistry.gatech.edu.

ORCID

Chen He: 0000-0001-5426-769X

Robert M. Dickson: 0000-0003-0042-6194

Jeffrey T. Petty: 0000-0003-0149-5335

Author Contributions

The manuscript was written through contributions of all authors. All authors have given approval to the final version of the manuscript.

Author Contributions

‖C.H., J.T.P.: These authors contributed equally.

Funding

We thank the National Science Foundation (CHE-1611451), National Institutes of Health (1R15GM102818), the Furman Advantage program, and the Vasser-Woolley Foundation. This work was supported in part by the National Science Foundation EPSCoR Program under NSF Award No. OIA-1655740. Any opinions, findings and conclusions or recommendations expressed in this material are those of the author(s) and do not necessarily reflect those of the National

DOI: 10.1021/acs.jpcc.9b03773
J. Phys. Chem. C 2019, 123, 17588−17597

Science Foundation. This work was also performed, in part, at the Center for Integrated Nanotechnologies, an Office of Science User Facility operated for the U.S. Department of Energy (DOE) Office of Science. Los Alamos National Laboratory, an affirmative action equal opportunity employer, is managed by Triad National Security, LLC, for the U.S. Department of Energy's NNSA, under contract 89233218CNA000001.

Notes

The authors declare no competing financial interest.

■ ACKNOWLEDGMENTS

We are grateful to the National Science Foundation for support of this work. We also thank Mr. Carter E. Edmunds for maintaining the mass spectrometer.

■ REFERENCES

(1) Kubo, R. Electronic Properties of Metallic Fine Particles. I. *J. Phys. Soc. Jpn.* **1962**, *17*, 975−986.
(2) Zheng, J.; Nicovich, P. R.; Dickson, R. M. Highly Fluorescent Noble-Metal Quantum Dots. *Annu. Rev. Phys. Chem.* **2007**, *58*, 409−431.
(3) Gell, L.; Kulesza, A.; Petersen, J.; Röhr, M. I. S.; Mitrić, R.; Bonačić-Koutecký, V. Tuning Structural and Optical Properties of Thiolate-Protected Silver Clusters by Formation of a Silver Core with Confined Electrons. *J. Phys. Chem. C* **2013**, *117*, 14824−14831.
(4) Weerawardene, K. L. D. M.; Häkkinen, H.; Aikens, C. M. Connections between Theory and Experiment for Gold and Silver Nanoclusters. *Annu. Rev. Phys. Chem.* **2018**, *69*, 205−229.
(5) de Heer, W. A. The Physics of Simple Metal Clusters: Experimental Aspects and Simple Models. *Rev. Mod. Phys.* **1993**, *65*, 611−676.
(6) Lecoultre, S.; Rydlo, A.; Félix, C. Efficient Trapping of Silver Cations in a Rare Gas Matrix: Ag_3^+ in Argon. *J. Chem. Phys.* **2007**, *126*, 204507.
(7) Harbich, W.; Fedrigo, S.; Meyer, F.; Lindsay, D. M.; Lignieres, J.; Rivoal, J. C.; Kreisle, D. Deposition of Mass Selected Silver Clusters in Rare Gas Matrices. *J. Chem. Phys.* **1990**, *93*, 8535−8543.
(8) Petty, J. T.; Zheng, J.; Hud, N. V.; Dickson, R. M. DNA-Templated Ag Nanocluster Formation. *J. Am. Chem. Soc.* **2004**, *126*, 5207−5212.
(9) Gwinn, E.; Schultz, D.; Copp, S.; Swasey, S. DNA-Protected Silver Clusters for Nanophotonics. *Nanomaterials* **2015**, *5*, 180−207.
(10) Obliosca, J. M.; Liu, C.; Batson, R. A.; Babin, M. C.; Werner, J. H.; Yeh, H.-C. DNA/RNA Detection Using DNA-Templated Few-Atom Silver Nanoclusters. *Biosensors* **2013**, *3*, 185−200.
(11) Goswami, N.; Zheng, K.; Xie, J. Bio-NCs − the Marriage of Ultrasmall Metal Nanoclusters with Biomolecules. *Nanoscale* **2014**, *6*, 13328−13347.
(12) Liu, J. DNA-Stabilized, Fluorescent, Metal Nanoclusters for Biosensor Development. *TrAC, Trends Anal. Chem.* **2014**, *58*, 99−111.
(13) Daune, M.; Kekker, C. A.; Schachman, H. K. Complexes of Silver Ion with Natural and Synthetic Polynucleotides. *Biopolymers* **1966**, *4*, 51−76.
(14) Jensen, R. H.; Davidson, N. Spectrophotometric, Potentiometric, and Density Gradient Ultracentrifugation Studies of the Binding of Silver Ion by DNA. *Biopolymers* **1966**, *4*, 17−32.
(15) Koszinowski, K.; Ballweg, K. A Highly Charged Ag_6^{4+} Core in a DNA-Encapsulated Silver Nanocluster. *Chem. - Eur. J.* **2010**, *16*, 3285−3290.
(16) O'Neill, P. R.; Velazquez, L. R.; Dunn, D. G.; Gwinn, E. G.; Fygenson, D. K. Hairpins with Poly-C Loops Stabilize Four Types of Fluorescent Ag_n:DNA. *J. Phys. Chem. C* **2009**, *113*, 4229−4233.
(17) Petty, J. T.; Fan, C.; Story, S. P.; Sengupta, B.; St. John Iyer, A.; Prudowsky, Z.; Dickson, R. M. DNA Encapsulation of 10 Silver Atoms Producing a Bright, Modulatable, Near-Infrared-Emitting Cluster. *J. Phys. Chem. Lett.* **2010**, *1*, 2524−2529.
(18) Petty, J. T.; Sergev, O. O.; Kantor, A. G.; Rankine, I. J.; Ganguly, M.; David, F. D.; Wheeler, S. K.; Wheeler, J. F. Ten-Atom Silver Cluster Signaling and Tempering DNA Hybridization. *Anal. Chem.* **2015**, *87*, 5302−5309.
(19) Schultz, D.; Gwinn, E. G. Silver Atom and Strand Numbers in Fluorescent and Dark Ag:DNAs. *Chem. Commun.* **2012**, *48*, 5748−5750.
(20) Choi, S.; Yu, J.; Patel, S. A.; Tzeng, Y.-L.; Dickson, R. M. Tailoring Silver Nanodots for Intracellular Staining. *Photochem. Photobiol. Sci.* **2011**, *10*, 109−115.
(21) Petty, J. T.; Sengupta, B.; Story, S. P.; Degtyareva, N. N. DNA Sensing by Amplifying the Number of Near-Infrared Emitting, Oligonucleotide-Encapsulated Silver Clusters. *Anal. Chem.* **2011**, *83*, 5957−5964.
(22) Ramazanov, R. R.; Sych, T. S.; Reveguk, Z. V.; Maksimov, D. A.; Vdovichev, A. A.; Kononov, A. I. Ag − DNA Emitter: Metal Nanorod or Supramolecular Complex? *J. Phys. Chem. Lett.* **2016**, *7*, 3560−3566.
(23) Richards, C. I.; Choi, S.; Hsiang, J.-C.; Antoku, Y.; Vosch, T.; Bongiorno, A.; Tzeng, Y.-L.; Dickson, R. M. Oligonucleotide-Stabilized Ag Nanocluster Fluorophores. *J. Am. Chem. Soc.* **2008**, *130*, 5038−5039.
(24) Copp, S. M.; Bogdanov, P.; Debord, M.; Singh, A.; Gwinn, E. Base Motif Recognition and Design of DNA Templates for Fluorescent Silver Clusters by Machine Learning. *Adv. Mater. (Weinheim, Ger.)* **2014**, *26*, 5839−5845.
(25) Petty, J. T.; Fan, C.; Story, S. P.; Sengupta, B.; Sartin, M.; Hsiang, J.-C.; Perry, J. W.; Dickson, R. M. Optically Enhanced, Near-IR, Silver Cluster Emission Altered by Single Base Changes in the DNA Template. *J. Phys. Chem. B* **2011**, *115*, 7996−8003.
(26) Yeh, H. C.; Sharma, J.; Han, J. J.; Martinez, J. S.; Werner, J. H. A DNA − Silver Nanocluster Probe That Fluoresces Upon Hybridization. *Nano Lett.* **2010**, *10*, 3106−3110.
(27) Petty, J. T.; Giri, B.; Miller, I. C.; Nicholson, D. A.; Sergev, O. O.; Banks, T. M.; Story, S. P. Silver Clusters as Both Chromophoric Reporters and DNA Ligands. *Anal. Chem.* **2013**, *85*, 2183−2190.
(28) Vosch, T.; Antoku, Y.; Hsiang, J.-C.; Richards, C. I.; Gonzalez, J. I.; Dickson, R. M. Strongly Emissive Individual DNA-Encapsulated Ag Nanoclusters as Single-Molecule Fluorophores. *Proc. Natl. Acad. Sci. U. S. A.* **2007**, *104*, 12616−12621.
(29) Richards, C. I.; Hsiang, J.-C.; Senapati, D.; Patel, S.; Yu, J.; Vosch, T.; Dickson, R. M. Optically Modulated Fluorophores for Selective Fluorescence Signal Recovery. *J. Am. Chem. Soc.* **2009**, *131*, 4619−4621.
(30) Hsiang, J.-C.; Fleischer, B. C.; Dickson, R. M. Dark State-Modulated Fluorescence Correlation Spectroscopy for Quantitative Signal Recovery. *J. Phys. Chem. Lett.* **2016**, *7*, 2496−2501.
(31) Eichhorn, G. L.; Butzow, J. J.; Clark, P.; Tarien, E. Interaction of Metal Ions with Polynucleotides and Related Compounds. X. Studies on the Reaction of Silver(I) with the Nucleosides and Polynucleotides, and the Effect of Silver(I) on the Zinc(II) Degradation of Polynucleotides. *Biopolymers* **1967**, *5*, 283−296.
(32) Ritchie, C. M.; Johnsen, K. R.; Kiser, J. R.; Antoku, Y.; Dickson, R. M.; Petty, J. T. Ag Nanocluster Formation Using a Cytosine Oligonucleotide Template. *J. Phys. Chem. C* **2007**, *111*, 175−181.
(33) Sengupta, B.; Ritchie, C.; Buckman, J.; Johnsen, K.; Goodwin, P.; Petty, J. Base-Directed Formation of Fluorescent Silver Clusters. *J. Phys. Chem. C* **2008**, *112*, 18776−18782.
(34) Ganguly, M.; Bradsher, C.; Goodwin, P.; Petty, J. T. DNA-Directed Fluorescence Switching of Silver Clusters. *J. Phys. Chem. C* **2015**, *119*, 27829−27837.
(35) Petty, J. T.; Ganguly, M.; Rankine, I. J.; Baucum, E. J.; Gillan, M. J.; Eddy, L. E.; Léon, J. C.; Müller, J. Repeated and Folded DNA Sequences and Their Modular Ag_{10}^{6+} Cluster. *J. Phys. Chem. C* **2018**, *122*, 4670−4680.
(36) Petty, J. T.; Ganguly, M.; Yunus, A. I.; He, C.; Goodwin, P. M.; Lu, Y.-H.; Dickson, R. M. A DNA-Encapsulated Silver Cluster and the

DOI: 10.1021/acs.jpcc.9b03773
J. Phys. Chem. C 2019, 123, 17588−17597

Roles of Its Nucleobase Ligands. *J. Phys. Chem. C* **2018**, *122*, 28382−28392.
(37) Bloomfield, V. A.; Crothers, D. M.; Tinoco, J. *Ignacio Nucleic Acids: Structures, Properties, and Functions*; University Science Books: Sausaltio, CA, 2000; p 794, Chapter 14.
(38) Manning, G. S. The Molecular Theory of Polyelectrolyte Solutions with Applications to the Electrostatic Properties of Polynucleotides. *Q. Rev. Biophys.* **1978**, *11*, 179−246.
(39) He, C.; Nguyen, T. D.; Edme, K.; Olvera de la Cruz, M.; Weiss, E. A. Noncovalent Control of the Electrostatic Potential of Quantum Dots through the Formation of Interfacial Ion Pairs. *J. Am. Chem. Soc.* **2017**, *139*, 10126−10132.
(40) Petty, J. T.; Story, S. P.; Juarez, S.; Votto, S. S.; Herbst, A. G.; Degtyareva, N. N.; Sengupta, B. Optical Sensing by Transforming Chromophoric Silver Clusters in DNA Nanoreactors. *Anal. Chem.* **2012**, *84*, 356−364.
(41) Crosby, G. A.; Demas, J. N. Measurement of Photoluminescence Quantum Yields. Review. *J. Phys. Chem.* **1971**, *75*, 991−1024.
(42) Lakowicz, J. R. *Principles of Fluorescence Spectroscopy*, 3rd ed.; Springer: New York, Berlin, 2006.
(43) Petty, J. T.; Sergev, O. O.; Nicholson, D. A.; Goodwin, P. M.; Giri, B.; McMullan, D. R. A Silver Cluster − DNA Equilibrium. *Anal. Chem.* **2013**, *85*, 9868−9876.
(44) Culbertson, C. T.; Jacobson, S. C.; Ramsey, J. M. Diffusion Coefficient Measurements in Microfluidic Devices. *Talanta* **2002**, *56*, 365−373.
(45) Lindahl, T.; Ljungquist, S.; Siegert, W.; Nyberg, B.; Sperens, B. DNA N-Glycosidases: Properties of Uracil-DNA Glycosidase from Escherichia Coli. *J. Biol. Chem.* **1977**, *252*, 3286−3294.
(46) Barsky, D.; Foloppe, N.; Ahmadia, S.; Wilson, D. M., 3rd; MacKerell, A. D., Jr. New Insights into the Structure of Abasic DNA from Molecular Dynamics Simulations. *Nucleic Acids Res.* **2000**, *28*, 2613−2626.
(47) Yergey, J.; Heller, D.; Hansen, G.; Cotter, R. J.; Fenselau, C. Isotopic Distributions in Mass-Spectra of Large Molecules. *Anal. Chem.* **1983**, *55*, 353−356.
(48) Schultz, D.; Gardner, K.; Oemrawsingh, S. S. R.; Markešević, N.; Olsson, K.; Debord, M.; Bouwmeester, D.; Gwinn, E. Evidence for Rod-Shaped DNA-Stabilized Silver Nanocluster Emitters. *Adv. Mater. (Weinheim, Ger.)* **2013**, *25*, 2797−2803.
(49) Hooley, E. N.; Carro-Temboury, M. R.; Vosch, T. Probing the Absorption and Emission Transition Dipole Moment of DNA Stabilized Silver Nanoclusters. *J. Phys. Chem. A* **2017**, *121*, 963−968.
(50) Sanborn, M. E.; Connolly, B. K.; Gurunathan, K.; Levitus, M. Fluorescence Properties and Photophysics of the Sulfoindocyanine Cy3 Linked Covalently to DNA. *J. Phys. Chem. B* **2007**, *111*, 11064−11074.
(51) Unruh, J. R.; Gokulrangan, G.; Lushington, G. H.; Johnson, C. K.; Wilson, G. S. Orientational Dynamics and Dye − DNA Interactions in a Dye-Labeled DNA Aptamer. *Biophys. J.* **2005**, *88*, 3455−3465.
(52) Knoppe, S.; Bürgi, T. Chirality in Thiolate-Protected Gold Clusters. *Acc. Chem. Res.* **2014**, *47*, 1318−1326.
(53) Rodger, A.; Norden, B. *Circular Dichroism and Linear Dichroism*; Oxford: New York, 1997.
(54) Swasey, S. M.; Karimova, N.; Aikens, C. M.; Schultz, D. E.; Simon, A. J.; Gwinn, E. G. Chiral Electronic Transitions in Fluorescent Silver Clusters Stabilized by DNA. *ACS Nano* **2014**, *8*, 6883−92.
(55) Petty, J. T.; Sergev, O. O.; Ganguly, M.; Rankine, I. J.; Chevrier, D. M.; Zhang, P. A Segregated, Partially Oxidized, and Compact Ag_{10} Cluster within an Encapsulating DNA Host. *J. Am. Chem. Soc.* **2016**, *138*, 3469−3477.
(56) Spiess, E.; Bestvater, F.; Heckel-Pompey, A.; Toth, K.; Hacker, M.; Stobrawa, G.; Feurer, T.; Wotzlaw, C.; Bercher-Pfannschmidt, U.; Porwal, T.; Acker, H. Two-Photon Excitation and Emission Spectra of the Green Fluorescent Protein Variants ECFP, EGFP and EYFP. *J. Microsc.* **2005**, *217*, 200−204.
(57) Cerretani, C.; Carro-Temboury, M. R.; Krause, S.; Bogh, S. A.; Vosch, T. Temperature Dependent Excited State Relaxation of a Red Emitting DNA-Templated Silver Nanocluster. *Chem. Commun.* **2017**, *53*, 12556−12559.
(58) Hsiang, J.-C.; Jablonski, A. E.; Dickson, R. M. Optically Modulated Fluorescence Bioimaging: Visualizing Obscured Fluorophores in High Background. *Acc. Chem. Res.* **2014**, *47*, 1545−1554.
(59) Sanden, T.; Persson, G.; Thyberg, P.; Blom, H.; Widengren, J. Monitoring Kinetics of Highly Environment Sensitive States of Fluorescent Molecules by Modulated Excitation and Time-Averaged Fluorescence Intensity Recording. *Anal. Chem.* **2007**, *79*, 3330−3341.
(60) Patel, S. A.; Cozzuol, M.; Hales, J. M.; Richards, C. I.; Sartin, M.; Hsiang, J.-C.; Vosch, T.; Perry, J. W.; Dickson, R. M. Electron Transfer-Induced Blinking in Ag Nanodot Fluorescence. *J. Phys. Chem. C* **2009**, *113*, 20264−20270.
(61) Zadeh, J. N.; Steenberg, C. D.; Bois, J. S.; Wolfe, B. R.; Pierce, M. B.; Khan, A. R.; Dirks, R. M.; Pierce, N. A. Nupack: Analysis and Design of Nucleic Acid Systems. *J. Comput. Chem.* **2011**, *32*, 170−173.
(62) Rivetti, C.; Guthold, M.; Bustamante, C. Scanning Force Microscopy of DNA Deposited onto Mica: Equilibration Versus Kinetic Trapping Studied by Statistical Polymer Chain Analysis. *J. Mol. Biol.* **1996**, *264*, 919−932.
(63) Silverman, A. P.; Kool, E. T. Detecting RNA and DNA with Templated Chemical Reactions. *Chem. Rev.* **2006**, *106*, 3775−3789.
(64) Percivalle, C.; Bartolo, J. F.; Ladame, S. Oligonucleotide-Templated Chemical Reactions: Pushing the Boundaries of a Nature-Inspired Process. *Org. Biomol. Chem.* **2013**, *11*, 16−26.
(65) Huber, K. P.; Herzberg, G. *Molecular Spectra and Molecular Structure. IV. Constants of Diatomic Molecules*; Van Nostrand Reinhold Company: Atlanta, GA, 1979; Vol. *IV*, p 716.
(66) Spasov, V. A.; Lee, T. H.; Maberry, J. P.; Ervin, K. M. Measurement of the Dissociation Energies of Anionic Silver Clusters (Ag_n^-, n = 2−11) by Collision-Induced Dissociation. *J. Chem. Phys.* **1999**, *110*, 5208−5217.
(67) Copp, S. M.; Schultz, D.; Swasey, S.; Pavlovich, J.; Debord, M.; Chiu, A.; Olsson, K.; Gwinn, E. Magic Numbers in DNA-Stabilized Fluorescent Silver Clusters Lead to Magic Colors. *J. Phys. Chem. Lett.* **2014**, *5*, 959−963.
(68) Petty, J. T.; Nicholson, D. A.; Sergev, O. O.; Graham, S. K. Near-Infrared Silver Cluster Optically Signaling Oligonucleotide Hybridization and Assembling Two DNA Hosts. *Anal. Chem.* **2014**, *86*, 9220−9228.
(69) Swasey, S. M.; Copp, S. M.; Nicholson, H. C.; Gorovits, A.; Bogdanov, P.; Gwinn, E. G. High Throughput near Infrared Screening Discovers DNA-Templated Silver Clusters with Peak Fluorescence Beyond 950 nm. *Nanoscale* **2018**, *10*, 19701−19705.
(70) Huard, D. J. E.; Demissie, A.; Kim, D.; Lewis, D.; Dickson, R. M.; Petty, J. T.; Lieberman, R. L. Atomic Structure of a Fluorescent Ag_8 Cluster Templated by a Multistranded DNA Scaffold. *J. Am. Chem. Soc.* **2019**, DOI: 10.1021/jacs.8b12203.
(71) Kerppola, T. K. Visualization of Molecular Interactions by Fluorescence Complementation. *Nat. Rev. Mol. Cell Biol.* **2006**, *7*, 449−456.
(72) Lin, C. Y.; Both, J.; Do, K.; Boxer, S. G. Mechanism and Bottlenecks in Strand Photodissociation of Split Green Fluorescent Proteins (GFPs). *Proc. Natl. Acad. Sci. U. S. A.* **2017**, *114*, E2146−E2155.
(73) Morris, F. D.; Peterson, E. M.; Heemstra, J. M.; Harris, J. M. Single-Molecule Kinetic Investigation of Cocaine-Dependent Split-Aptamer Assembly. *Anal. Chem.* **2018**, *90*, 12964−12970.
(74) Obliosca, J. M.; Babin, M. C.; Liu, C.; Liu, Y. L.; Chen, Y. A.; Batson, R. A.; Ganguly, M.; Petty, J. T.; Yeh, H. C. A Complementary Palette of Nanocluster Beacons. *ACS Nano* **2014**, *8*, 10150−10160.
(75) Peng, M.; Na, N.; Ouyang, J. A Fluorescence Light-up Silver Nanocluster Beacon Modulated by Metal Ions and Its Application in Telomerase-Activity Detection. *Chem. - Eur. J.* **2019**, *25*, 3598−3605.
(76) Juul, S.; Obliosca, J. M.; Liu, C.; Liu, Y.-L.; Chen, Y.-A.; Imphean, D. M.; Knudsen, B. R.; Ho, Y.-P.; Leong, K. W.; Yeh, H.-C.

DOI: 10.1021/acs.jpcc.9b03773
J. Phys. Chem. C 2019, 123, 17588−17597

Nanocluster Beacons as Reporter Probes in Rolling Circle Enhanced Enzyme Activity Detection. *Nanoscale* **2015**, *7*, 8332−8337.
(77) Chen, Y.-A.; Vu, H. T.; Liu, Y.-L.; Chen, Y.-I.; Nguyen, T. D.; Kuo, Y.-A.; Hong, S.; Chen, Y.-A.; Carnahan, S.; Petty, J. T.; Yeh, H.-C. Improving Nanocluster Beacon Performance by Blocking the Unlabeled NC Probes. *Chem. Commun.* **2019**, *55*, 462−465.
(78) Petty, J. T.; Ganguly, M.; Rankine, I. J.; Chevrier, D. M.; Zhang, P. A DNA-Encapsulated and Fluorescent Ag_{10}^{6+} Cluster with a Distinct Metal-Like Core. *J. Phys. Chem. C* **2017**, *121*, 14936−14945.
(79) Lippert, B.; Sanz Miguel, P. J. The Renaissance of Metal − Pyrimidine Nucleobase Coordination Chemistry. *Acc. Chem. Res.* **2016**, *49*, 1537−1545.
(80) Day, H. A.; Huguin, C.; Waller, Z. A. E. Silver Cations Fold i-Motif at Neutral pH. *Chem. Commun.* **2013**, *49*, 7696−7698.
(81) Kondo, J.; Tada, Y.; Dairaku, T.; Hattori, Y.; Saneyoshi, H.; Ono, A.; Tanaka, Y. A Metallo-DNA Nanowire with Uninterrupted One-Dimensional Silver Array. *Nat. Chem.* **2017**, *9*, 956−960.
(82) Swasey, S. M.; Leal, L. E.; Lopez-Acevedo, O.; Pavlovich, J.; Gwinn, E. G. Silver(I) as DNA Glue: Ag^{+}-Mediated Guanine Pairing Revealed by Removing Watson-Crick Constraints. *Sci. Rep.* **2015**, *5*, 10163.
(83) Ono, A.; Cao, S.; Togashi, H.; Tashiro, M.; Fujimoto, T.; MacHinami, T.; Oda, S.; Miyake, Y.; Okamoto, I.; Tanaka, Y. Specific Interactions between Silver(I) Ions and Cytosine-Cytosine Pairs in DNA Duplexes. *Chem. Commun.* **2008**, 4825−4827.
(84) Volkov, I. L.; Reveguk, Z. V.; Serdobintsev, P. Y.; Ramazanov, R. R.; Kononov, A. I. DNA as UV Light−Harvesting Antenna. *Nucleic Acids Res.* **2018**, *46*, 3543−3551.
(85) Mistry, L.; El-Zubir, O.; Dura, G.; Clegg, W.; Waddell, P. G.; Pope, T.; Hofer, W. A.; Wright, N. G.; Horrocks, B. R.; Houlton, A. Addressing the Properties of "Metallo-DNA" with a Ag(I)-Mediated Supramolecular Duplex. *Chem. Sci.* **2019**, *10*, 3186−3195.
(86) Müller, J. Metal-Mediated Base Pairs in Parallel-Stranded DNA. *Beilstein J. Org. Chem.* **2017**, *13*, 2671−2681.
(87) Copp, S. M.; Schultz, D.; Swasey, S. M.; Faris, A.; Gwinn, E. G. Cluster Plasmonics: Dielectric and Shape Effects on DNA-Stabilized Silver Clusters. *Nano Lett.* **2016**, *16*, 3594−3599.
(88) Ramazanov, R. R.; Kononov, A. I. Excitation Spectra Argue for Threadlike Shape of DNA-Stabilized Silver Fluorescent Clusters. *J. Phys. Chem. C* **2013**, *117*, 18681−18687.

DOI: 10.1021/acs.jpcc.9b03773
J. Phys. Chem. C 2019, 123, 17588−17597